Dual modality ECT-MIT multi-phase flow imaging

M Zhang, L Ma, M Soleimani

Engineering Tomography Lab (ETL), Department of Electronic and Electrical Engineering, University of Bath, UK. m.soleimani@bath.ac.uk

ABSTRACT-Three-phase flow imaging is a very challenging problem in industrial process tomography. A particular interest here is three phase flow including both conductive and non-conductive phases. Currently there is no robust solution to this problem. Electrical capacitance tomography (ECT) has been applied to visualise the permittivity distribution by measuring inter-capacitance between electrodes around sensing area. Magnetic inductance tomography (MIT) is a technique to image the conductivity distribution through the inductance measurements over the coils around the sensing area. In this paper, the three-phase flow is classified into two scenarios: air background and water background. A dual-modality method of ECT and MIT is proposed to image both the conductive and dielectric components under test. As a result of this experiment, the dual-modality method is able to solve air-background three-phase flow imaging, but a problem has been raised in the water-background scenario. The static experiment results are promising for such contactless three phase flow imaging.

Keywords: dual modality, ECT, MIT, high contrast, flow imaging, static experiment

1. Introduction

Electrical capacitance tomography (ECT) and magnetic inductance tomography (MIT) have been known as non-destructive and non-invasive testing methods to visualize the distribution of permittivity and conductivity respectively. ECT visualizes the permittivity changes in specified sensing area by processing the capacitance measurements between electrodes on different time. Currently it is a relatively mature technique on multi-phase flow imaging [1, 2] and the application of ECT includes monitoring gas-solid flows in pneumatic conveyors and gas-oil in oil pipeline [3, 4]. MIT is a technique to image the conductivity distribution through the inductance measurements over the coils around the sensing area. the applications of multi-phase flow imaging on MIT has studied by [5] and [6]. The applications of MIT for the industry processing imaging are still very challenging and so it is not very well established the same as ECT. There is not a robust and real time MIT data acquisition for low conductivity industrial process applications reported yet. The phase accuracy required for MIT low conductivity imaging poses a challenge in electronic hardware design of MIT as well as its shielding and sensor front end. The forward problem in MIT is a complex eddy current problem compared to well-understood elliptic partial differential equations describing the ECT forward modelling. Here we propose to use MIT as a complementary technique for the ECT in a sequential data fusion scheme.

In [7], electrical impedance methods has been used in the three-phase flow measurement to provide electric resistance and capacitance for calculating the oil, gas and water fractions. Normally the three-phase flow is mixture of gas, oil and water. The relative permittivity of each phase are different: $\varepsilon_{gas} \approx 1$, $\varepsilon_{oil} \approx 2-3$ and $\varepsilon_{water} \approx 80$. The permittivity difference is very small between gas and oil but very large between water and gas or oil. Therefore, this becomes a high-contrast problem of ECT imaging in distinguishing oil from gas. In addition

the electrical conductivity of the water phase will be a challenge for ECT modelling. In petroleum industry, to decrease the difficulty of three-phase flow, a separator is used to free the gas and the rest two-phase flow of oil and water is monitored. To provide a solution to determine the fraction of each phase without using a separator, which would saves cost on a separator, some dual-modality tomography are proposed. In [8, 9], electrical resistance tomography (ERT) is combined with ECT as a dual-modality solution. ERT generates an image that can discriminate gas (i.e. low conductivity) from mixture of oil and water (i.e. higher conductivity than gas), meanwhile an image from ECT distinguish water (i.e. high permittivity) from the mixture of gas and oil (i.e. low permittivity). And in [10, 11], the gamma radiation meter (GRM) are introduced to determine the fraction of gas from liquid (i.e. water and oil), similar to what is obtained from ERT. Then by fusing the images from ERT or GRM with ECT images, the distribution of three-phase flow is visualized. The data fusion method used in these dual-modalities is basically to merge the two separate images from ECT and ERT reconstruction. However ERT needs electrical contact between the sensors and the sample under test, and GRM takes a long time for measurement acquisition. By contrast, both ECT and MIT have advantages of no direct contact to the sample under test and fast speed on data acquisition and image reconstruction.

The dual modality of MIT-ECT is firstly introduced in [12], where an MIT guided ECT modality is proposed to solve the problem of effect from the grounded conductor in ECT. Unlike the data fusion used in ERT-ECT, MIT-ECT works in a sequential process. MIT is a method to obtain the information of the conductive water and to feed the information to the forward model of ECT, since the water with conductivity is also of high permittivity. The prior information helps to linearize the high contrast problem in ECT by producing a reference measurement (model) closer to the two low permittivity phases. Then ECT will image the rest parts in the sensing area. The focus of this paper is mainly to solve high contrast ECT problem aided by MIT, and that is currently being extended to imaging conductive background where major modification in ECT software will be needed.

2. Imaging modality

2.1 Forward problem

The forward problems of electromagnetic tomography are solved by the Maxwell's equations, Assuming that the time-harmonic fields with angular frequency ω is implemented to the Maxwell's equations. Due to low frequency tomography, the propagation effect is ignored [13]:

$$\nabla \times H = (\sigma + i\omega\varepsilon)E + J_s \tag{1}$$

$$\nabla \times E = -i\omega\mu H \tag{2}$$

$$\nabla \cdot B = 0 \tag{3}$$

$$\nabla \cdot D = 0 \tag{4}$$

where H is the magnetic field, E is the electric field, B is the magnetic flux, D is the electric displacement, , J_s is the electric current density. μ, ε and σ are the permeability, permittivity and conductivity respectively.

2.1.1 Forward problem in ECT

A typical ECT sensor usually consists of 8 or 12 electrodes, which is designed to measure the capacitance of the material under test [14]. And in a measurement, one of the electrodes is excited by a given voltage and the rest electrodes are grounded to receive signal of current. Outside of an ECT sensor, normally a screening wall is used to shield the effect from external electric field. From Maxwell's equations, the relationship between permittivity and conductivity distribution $\varepsilon(x)$, $\sigma(x)$and electrical potential $u(x)$are in the following way within the region, where

$$\nabla \cdot \left[\varepsilon(x) + \frac{\sigma(x)}{i\omega}\right] \nabla u(x) = 0 \tag{5}$$

And the boundary conditions of this problem are the electric potential $u(x)$ on different surfaces of the sensors.

$$u(x) = V \qquad on\ \Gamma_{\text{excited}} \tag{6}$$

$$u(x) = 0 \qquad on\ \Gamma_{Screening}\ and\ \Gamma_{unexcited} \tag{7}$$

where V is the excitation voltage, Γ_{excited} is the surface of the excited electrode, $\Gamma_{Screening}$ is the surface of the screening and $\Gamma_{unexcited}$ is the surface of the unexcited electrodes. The electric charge on the l-th electrode is generated from the Gauss's law, as shown below.

$$Q_l = -\int_{\Gamma_l} \left[\varepsilon(x) + \frac{\sigma(x)}{i\omega}\right] \frac{\partial u(x)}{\partial n} d\Gamma \tag{8}$$

where $\mathbf{n}$ is the normal vector on an electrode. This leads to a complex capacitance measurement, which has information about both electrical conductivity and dielectric permittivity. The sensitivity of this complex capacitance (if it can be measured), to each of these two electrical properties depends on our ability to measure accurately real and imaginary parts of the capacitance as well as operational frequency.

2.1.2 Forward problem in MIT

The governing equations for the quasi-static electromagnetic fields can be expressed in time-harmonic format below, where the displacement current is neglected [14]:

$$\nabla \times \left[\left(\frac{1}{\mu}\right) \nabla \times A\right] + i\omega(\sigma + i\omega\varepsilon)A + (\sigma + i\omega\varepsilon)\nabla V = J \quad (9)$$

$$i\omega\nabla \cdot (\sigma + i\omega\varepsilon)(A + \nabla V) = 0 \quad (10)$$

where A is magnetic vector potential, V is electric scalar potential, J is excitation current density, ω is angular frequency of the excitation current, μ is magnetic permeability. The induced voltages in sensing coils can then be calculated from results of the forward problem.

2.2 Inverse problem

To convert the measurements into an image of permittivity or conductivity distribution, we need reconstruction algorithms to solve this inverse problem. Iterative Tikhonov is an algorithm to solve ill-posed inverse problems [15]. The iteration function can be expressed as:

$$X_{k+1} = X_k + (S_k^T S_k + \gamma I)^{-1} S_k^T (M - SX_k) \quad (11)$$

where X_k is the k-th iteration of electrical properties of material under test, it can be permittivity for ECT or conductivity for MIT. S is the sensitivity map, and M is measurements. Then this iteration starts from an initial point X_0, and the rate of converging is controlled by the factor γ.

The sensitivity map, S, is the connection between the change of the measurement and the change of electrical passive parameters (μ, σ and ε), so the reconstruction is based on this map. This sensitivity equation has been studied in [16, 17], and it is generated from the equation below for both two tomograms.

$$\int_\Gamma \delta E_1 \times H_2 \cdot n \, d\Gamma = \int_\Omega [-i\omega\delta\mu H_1 H_2 + (\delta\sigma + i\omega\delta\varepsilon) E_1 E_2] \, d\Omega \quad (12)$$

Equation (12) provides a general form of sensitivity analysis that applies to ERT, ECT and MIT where E_1 and H_1 are electric and magnetic field with excitation number 1 (electrode or coil) and E_2 and H_2 are electric and magnetic field with excitation number 2 (electrode or coil). This formulation allows a change in boundary data (surface components and their surface integrals) to a change in material properties approximated by the volume integral of internal fields.

2.3 Improve reference point for ECT reconstruction

To reconstruct ECT images, the key inputs to the inverse solvers are the sensitivity map and the differences between measurements. And these two inputs are related to the selection of reference point. If oil and water samples are placed into an air-filled ECT sensor, then the relation between measurements, sensitivity maps and permittivity distribution is expressed in Figure 1.

C_{air}:	**The capacitance measurements of air-filled sensor**	ε_{air}:	**The permittivity distribution of air-filled sensor**
$C_{air+water}$:	**The capacitance measurements of the sensor containing air and water**	$\varepsilon_{air+water}$:	**The permittivity distribution of air and water**
$C_{air+water+oil}$:	**The capacitance measurements of the sensor containing air, water and oil**	$\varepsilon_{air+water+oil}$:	**The permittivity distribution of air, water and oil**
S_{air}:	**The sensitivity map of air-filled sensor**	$S_{air+water}$:	**The sensitivity map of air and water**

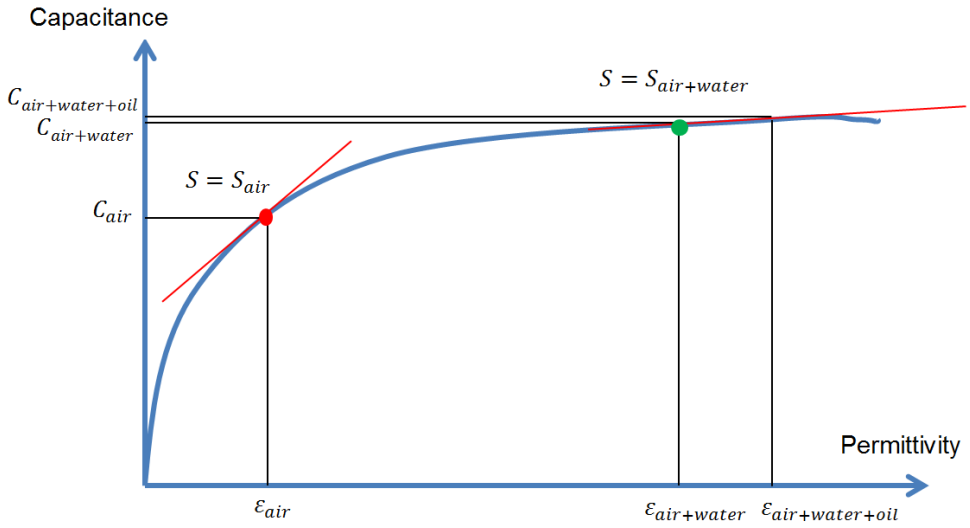

Figure 1. The non-linear relationship between capacitance and permittivity in ECT (air-background)

The schematic way of non-linear relationship between capacitance and permittivity in ECT is extended from [18]. Normally to detect an unknown distribution in ECT, the empty sensor is used at a reference point, i.e., the red point, where the sensitivity map S_{air} and capacitance measurement C_{air} is obtained from a purely air-filled sensor. In a multi-phase problem, to image the rest two phases within the ECT sensor is hard, since water is of high permittivity and increases non-linearity in reconstruction. To linearize the problem, a reference point include the water phase is selected. Instead of the red point, the green point contains the information of both air and water is closer to the real distribution and assists the inverse solver to find the oil phase easier.

The capacitance measurements for the green or red points are obtained straight from measurement machine. To investigate the changes in sensitivity maps, the three phases are categorized into two basic and simplified scenarios: **1. Air background**, where a bottle of water is inserted; **2. Water background**, where a bottle of air is inserted. In 0, the sensitivity maps between a pair of opposite electrodes are plotted. This ECT model is made of 12 electrodes, which evenly mounted on periphery of a pipe wall (relative permittivity of wall is $\varepsilon_{wall} \approx 3$). And the external radius of the pipe is in 100mm, and the thickness is 5mm, and the radius of the bottle is 29mm.

For air background, the sensitivity increases on the region of a bottle of water; but it decreases on the region of a bottle of air for water-background case. In Table 1, both the colour and the height on z-axis indicate the value of sensitivity. Those images show the change in sensitivity. This will help to find the third phase of oil in a three-phase problem.

The water in the three-phase problem is not only of high permittivity but also of conductivity. So MIT is introduced to image the conductive water from air and oil before ECT senses the unknown region to obtain the green point in Figure 1. Thereafter ECT utilizes the new information of water from MIT to shift the linearizing point from red to green. And the ECT reference data is also changed from the measurements of the air-filled sensor to the measurements of the sensor containing both air and water. At the final stage, the capacitance measurement of air, water and oil is processed to visualize the oil component.

	Air-background	
	Free space	A bottle of water sits in the sensor
Schematic diagram	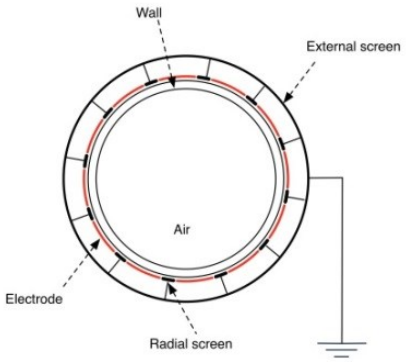	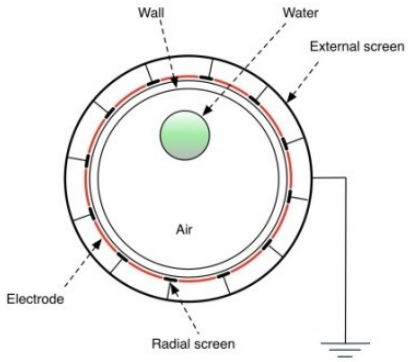
Sensitivity map of sensing region	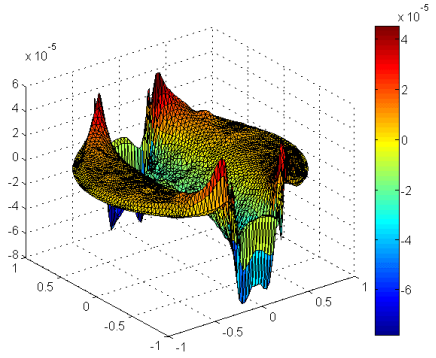	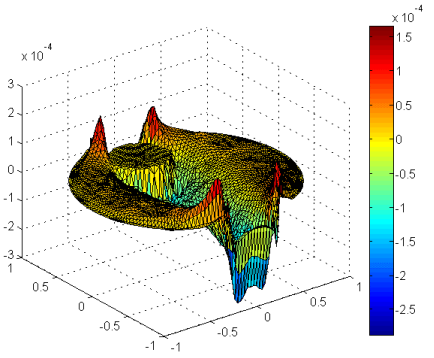
	Water-background	
	Fully water-filled sensor	A bottle of air sits in the water-filled sensor
Schematic diagram	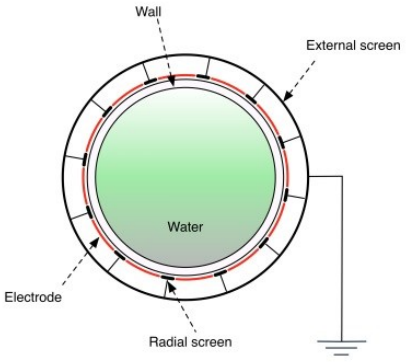	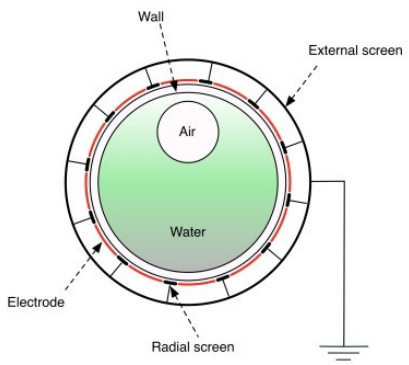
Sensitivity map of sensing region	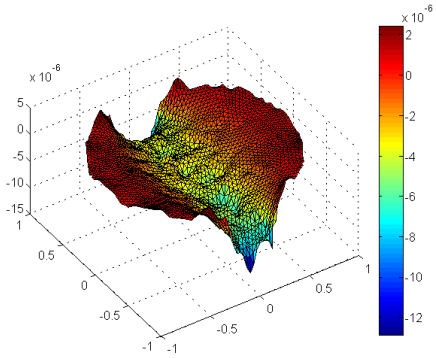	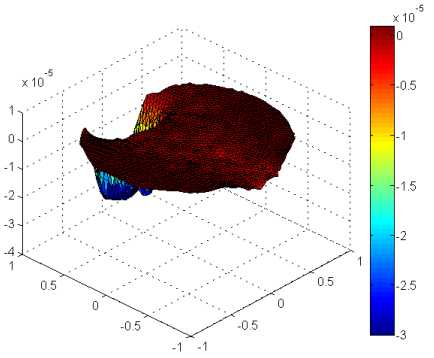

Table 1. The sensitivity maps between two opposite electrodes in the ECT sensor

2.4 Sequential dual modality procedure

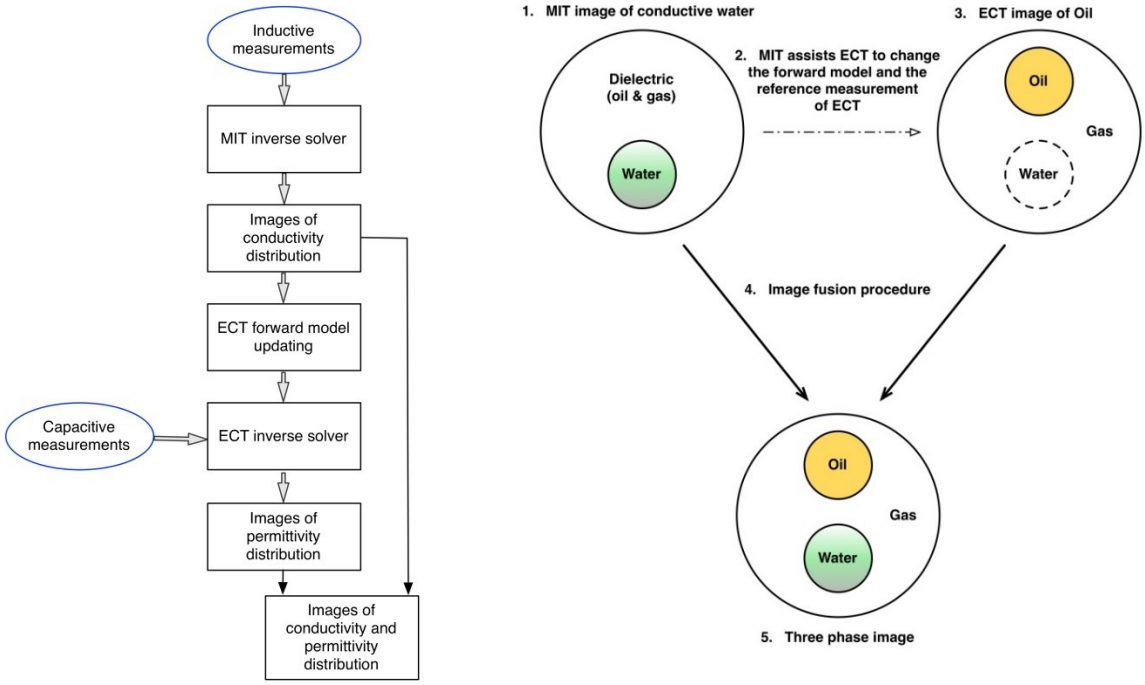

Figure 2. (a) Working flow chart of dual-modality; (b) Fusion of the two tomograms

Firstly in MIT system, by solving the difference in inductive measurements, an image of conductivity distribution is reconstructed, as shown in the step 1 of Figure 2(b). The ECT forward model and the set of capacitance measurements under this condition are acquired for this sequential procedure. To update the forward model, we assign the relative permittivity of 80 to the designated region of water in ECT forward model. To obtain the capacitance measurement, we replace the experiment samples according to the images got from MIT and collect the measurement.

Then ECT reconstructs permittivity distribution of the rest area apart from the water, therefore the oil and gas phase can be discriminated. The final stage is to merge the two images and generate a three-phase image. This procedure is also explained in the flow chart, Figure 2(a) and the fusion of the two tomograms are shown in Figure 2(b).To be noticed, MIT uses the inductive measurement and sensitivity map of air-filled MIT sensor as the reference point to find the conductive water component.

3. Setting up of experiments and simulation

3.1 Equipment description

	
(a) MIT sensor	(b) MIT measurement unit

Table 2. MIT sensor and measurement unit

The Bath MIT system consists of a coil array of equally spaced 16 air-core sensors, a National Instrument (NI) based data acquisition system and a host computer (Table 2 a and b). The sensing zone has a diameter of 25*cm*. Each coil has 6 turns, a side length of 1*cm*, and a radius of 2*cm*. The coil resonance frequency is 45*MHz*. This system was designed to measures the phase change caused by imaging substances and uses that change for image reconstruction. Among 16 coils, 8 coils are dedicated for transmitting signals, and the remaining 8 coils are used for receiving signals. The total number of independent measurements is therefore 64. Noting that the neighbouring measurements are eliminated to reduce the capacitive coupling effect between the excitation and receiving coils, therefore 48 measurements are used in the inverse model to passively map the distributions of the imaging subject. Furthermore, this system operates in MHz range in attempt to increase the signals, a common practice for MIT systems designed for biomedical and industrial process applications. Low frequency MIT can only be used for imaging highly conductive metallic samples. The detailed measurement system design has been reported in [19]. Inside the sensor, a circular tank is used to hold water for future experiment. The external diameter of the tank is 20*cm* with a thickness of 0.5*cm*.

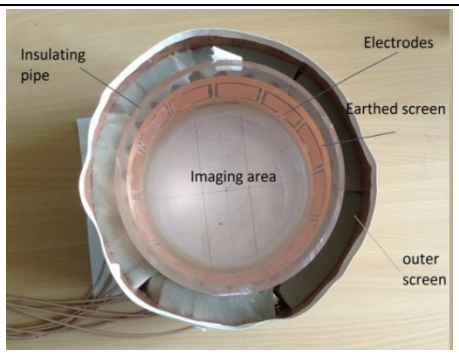	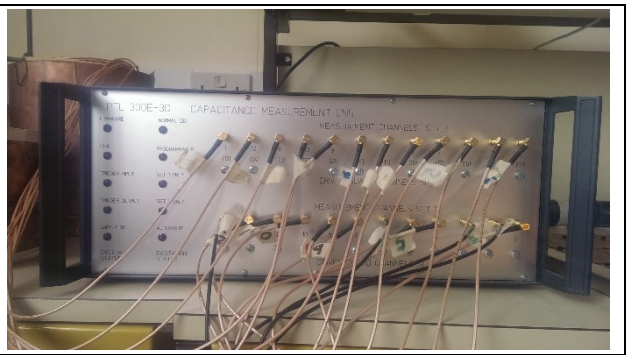
(c) ECT sensor	(d) ECT measurement unit

Table 3. ECT sensor and measurement unit

The ECT sensor consists of 12 copper electrodes mounted on the pipe of the same size as the tank in the MIT sensor. Each electrode in the size of 45*mm**40*mm* is evenly distributed on the periphery. For the purpose of screening, there is a thin piece of copper between neighbour electrodes and two circular strips of copper are separately mounted above and below the sensing electrodes. The ECT measurement system in our laboratory is the PTL 300E-3D from PROCESS TOMOGRAPHY LTD. It works in a fixed excitation frequency of 1.25 *MHz* and the minimum measurable capacitance is 0.3*fF*.

In our static experiments, bottles of saline water ($\varepsilon_{water} \approx 80$), silicone oil ($\varepsilon_{oil} = 2.5$) and air ($\varepsilon_{air} = 1$), are samples to simulate the three-phase flow. The radius of bottle is 29*mm*.

3.2 Simulation for conductivity in ECT

In section 4&5, experiments conducted in the two scenarios (i.e., air or water background) attempt to tell the feasibility and the limitation of each tomographic modality and the combined dual modalities. Generally, ECT is designed to test the dielectric material, but in our experiment the conductivity is introduced, as it is factor from the water component in three-phase flow. Therefore before applying ECT to the scenario of conductive water, the impact of conductivity on capacitance measurement should be investigated by both simulations and experiments.

In our experiments, sodium chloride (NaCl) is added into water to increase the conductivity, the permittivity of the solution changes as well. In [20], the permittivity changing as the concentrations changing in NaCl solution has been elaborated. And from [20], the relative permittivity change drops from 80.5 to 78.3 when we increase the concentration of saline water from 0 to 50*g/L* at 20°*C*. Since the permittivity change is very small within the concentration range of our experiments, the relative permittivity of water is fixed at 80 while the conductivity increases in our forward model.

The simulation of ECT is based on a noise-free complex-permittivity model. As shown in equation (5), the conductivity is the imaginary part of the complex permittivity. All of the bottles used in the simulation are 29*mm* in radius, and the sensor pipe is 100mm in external radius and 95*mm* in internal radius. The relative permittivity of the sensor pipe is 3. To match the real experiment, the simulation model works in the same frequency as the PTL 300E-3D equipment, which is f=1.25*MHz*.

4. Air Background

4.1 Impact of conductivity on capacitance measurement

4.1.1 Simulation results

A bottle of water standing in the centre of the sensor is measured as the reference. A bottle of oil is placed at (0*mm*, 65*mm*) for the sample measurement. While increasing the conductivity of water from 0 to 5 *S/m* in both cases, the capacitances data are collected. In each single set of capacitance measurements, there are 66 capacitances between 12 electrodes. And the measurements are in complex value. To indicate the trend of capacitance change, the 2-norm values of each set of 66 capacitances are used. In the third row of Table 4, the difference between the two measurements is $\|C_s - C_r\|_2$, which means the norm value is obtained after the subtraction.

Reference measurement $\|C_r\|_2$	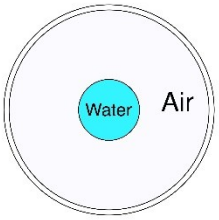	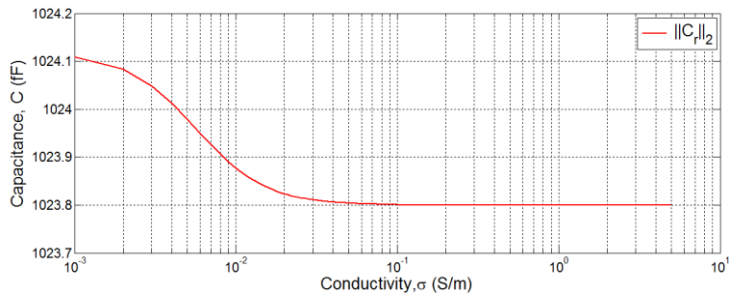
Sample measurement $\|C_s\|_2$	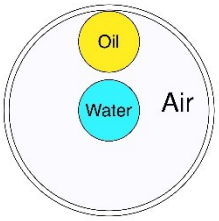	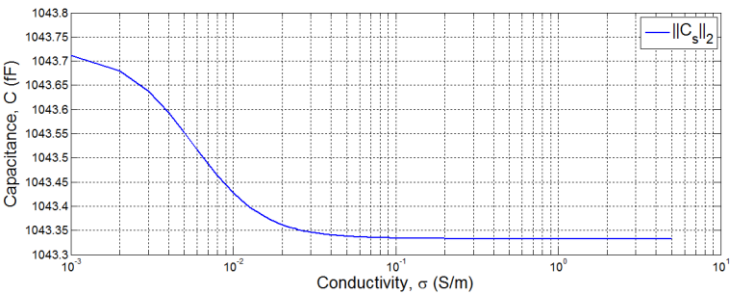
Difference of the measurements above $\|C_s - C_r\|_2$	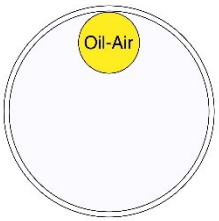	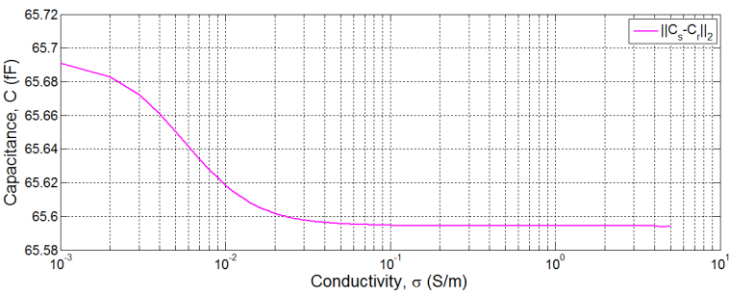

Table 4. 2-norm of simulated capacitance changes when conductivity increases from 0 to 5 *S/m* (air background)

From the simulation, the capacitance value changes in a small range: from 1023.8 to 1024.1 for reference measurement, from 1043.3 to 1043.7 for oil and water measurement. The capacitance change, i.e. the difference of two measurements, is the input for ECT reconstruction. The increasing conductivity causes small effect on the capacitance difference

from 65.59 to 65.69. According to the simulation of air background, the interference from a bottle of conductive water is very small for the ECT testing. Therefore, the conductivity in air background does not affect the capacitance measurement.

4.1.2 Experiment results

The simulation indicates that the conductivity of the water in a bottle makes a minor impact on the capacitance measurement. Experimentally, several bottles filled with saline solution of different concentration are individually placed in the centre of the sensor and the data of capacitances is measured. Table 5 are conductivities of different solutions measured by the Jenway 4510 conductivity meter. The bottle is placed in the centre of the sensor, and the according capacitances are measured. The outer radius of the bottle is 29mm. The capacitance change from DI water is plotted out in Figure 3. In Figure 4, the 2-norm values of capacitances of different solutions are listed.

Test material	Conductivity
9g/L saline solution	1.557 *S/m*
30g/L saline solution	4.68 *S/m*
50g/L saline solution	7.07 *S/m*
Tap water	0.0586 *S/m*
DI water	0.0003 *S/m*

Table 5. Conductivity of different solutions

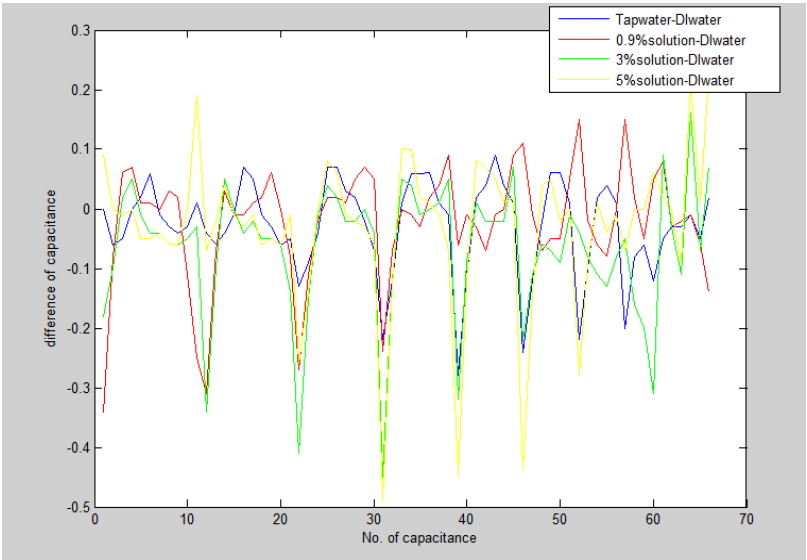

Figure 3. The plot of capacitance differences from DI water

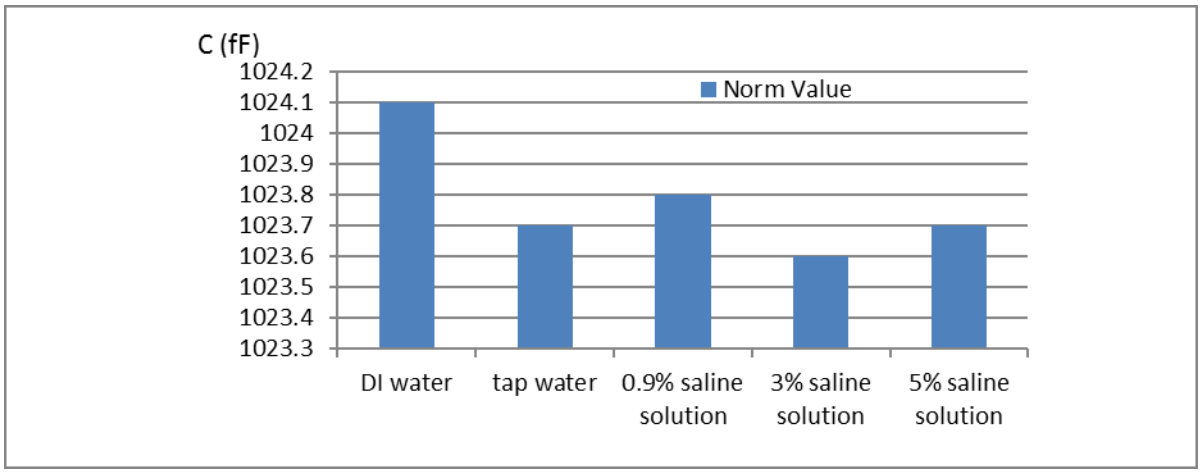

Figure 4. The 2-norm value of each set of measurements

Figure 4 indicates the minor impact of conductivity on the capacitance measurements, which matches the simulation. These results help us to move forward to next step of ECT experiments.

4.2 Dual modality test

4.2.1 Positions and concentration of samples in air

In the experiment, we use the 3% and 5% saline solution and the silicone oil as our samples. Each time, only two bottles are placed in the sensor: one filled with saline solution and the other filled with silicone oil. The position arrangement of the samples is shown in Table 6. In position 1, one bottle sits at top of coordinate (0*mm*, 65*mm*) and the other sits at bottom of coordinate (0*mm*, -65*mm*). In position 2&3, one bottle sits at centre (0*mm*, 0*mm*), the other is placed at top of coordinate (0*mm*, 65*mm*).

Position 1	Position 2	Position 3
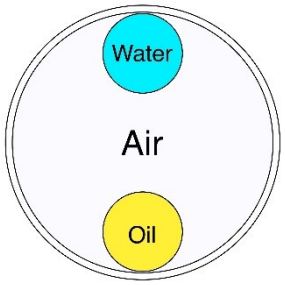	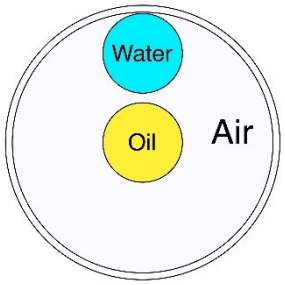	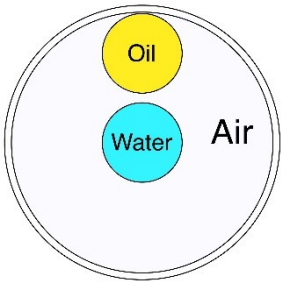

Table 6. Positions of the samples in air

4.2.2 MIT experiments

	Position 1 & 2	Position 3
3% saline solution	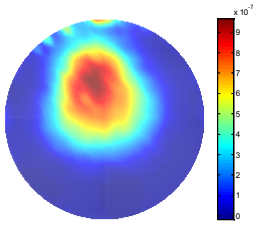	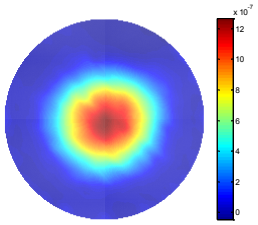
5% saline solution	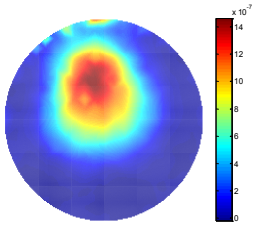	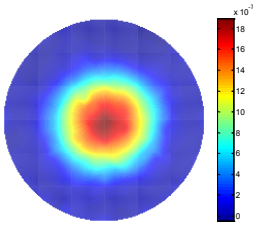

Table 7. MIT images of different position and concentrations of saline solution

The conductivity of both oil and air is closed to zero, so the major detectable component in MIT is the saline solution. Therefore in both case of Position 1 and 2, the images are the same. The experiment results are shown in Table 7.

4.2.3 ECT experiments

By obtaining the MIT results, the position and size information will be inputted to the ECT forward mode. In current stage of study, we only feed the position information to the ECT forward model, and set the water component as a circular region of diameter 56mm. After that, ECT reconstructs the rest sensing area excluding the water. The ECT experiment results are listed in Table 8. The images shown are the permittivity distribution. When MIT information is introduced into the ECT, the conductive component (i.e. water) is not visualized in the ECT images. To obtain a complete image of the three components, MIT and ECT images will be merged. In Table 8, the DI water is used as a reference sample to be compared with the conductive water. The non-conductivity of DI water disables the detection of MIT. Therefore, "N/A"s in the table mean that MIT-ECT cannot be applied to the completely non-conductive samples.

Position number	Modality	DI water & oil	3%saline solution & oil	5%saline solution & oil
1  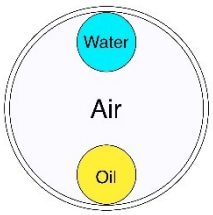	ECT	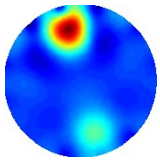	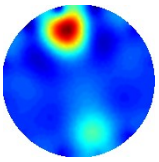	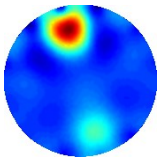
	MIT-ECT	N/A	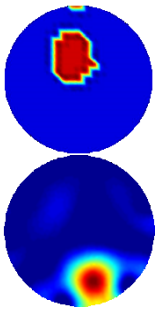	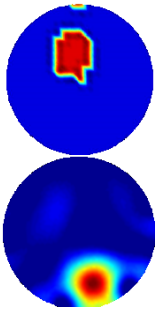
2  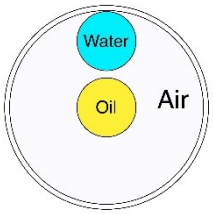	ECT	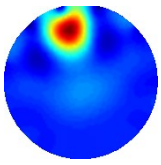	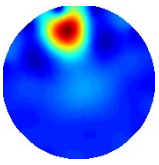	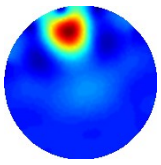
	MIT-ECT	N/A	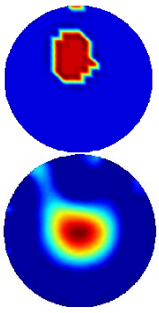	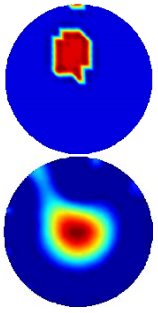
3  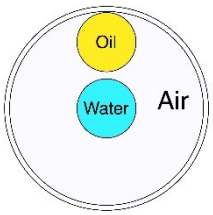	ECT	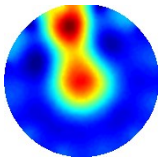	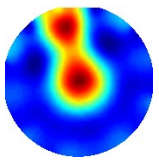	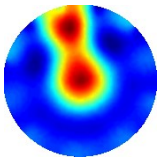
	MIT-ECT	N/A	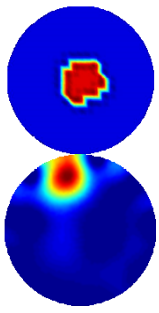	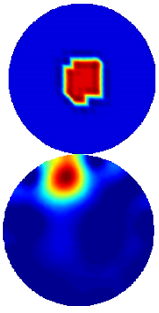

Table 8. The images from ECT-only and MIT-ECT system

ECT is able to distinguish the high permittivity from the low. When both the oil and the water sit near the electrodes, the reconstruction images tell the different permittivity of oil and water. However, when the water and the oil are placed closely together, the information from the images become difficult to read: (a) when the oil is facing the electrode, the image cannot

distinguish which is of higher permittivity; (b) when the water is facing the electrode, the oil placed in the middle can hardly be recognized from the ECT image. MIT helps to find the low conductive components (i.e. the saline solution), which provides prior information to assists ECT to image the rest region in the sensing area. With the help of MIT, ECT can distinguish the oil from the air, even though the water is closed to the oil. In Table 8, on the rows of **MIT-ECT**, the images on the top are the MIT images of the water inclusion, which is obtained by apply a threshold of 70% to the images in Table 7.The MIT-ECT dual-modality provides a better solution to separate oil from water in the three-phase flow imaging than ECT-only.

5. Water background

5.1 Impact of conductivity on capacitance measurement

5.1.1 Simulation results

Firstly, the sensor region is filled with water, where the capacitances measured are the reference measurements, C_r. Then a bottle of air and a bottle of oil are placed in our simulation model, where the sets of capacitances measured are the sample measurements, C_s. The 2-norm values of each set of 66 capacitance measurements are plotted along the conductivity change in the table below.

Reference measurements $\|C_r\|_2$	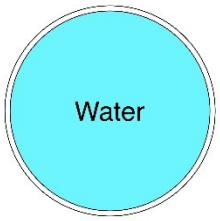	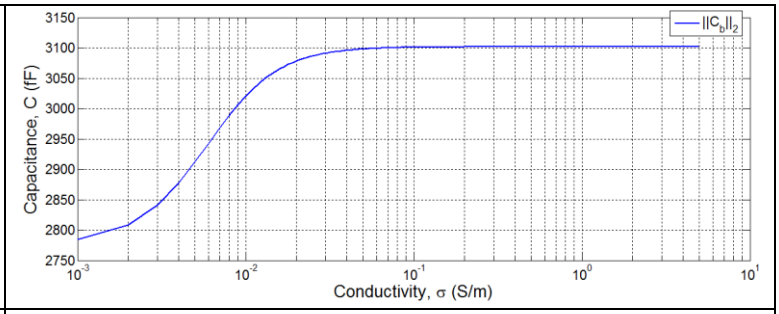
Sample measurements $\|C_s\|_2$	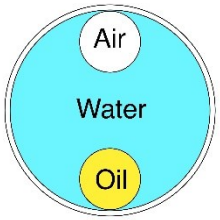	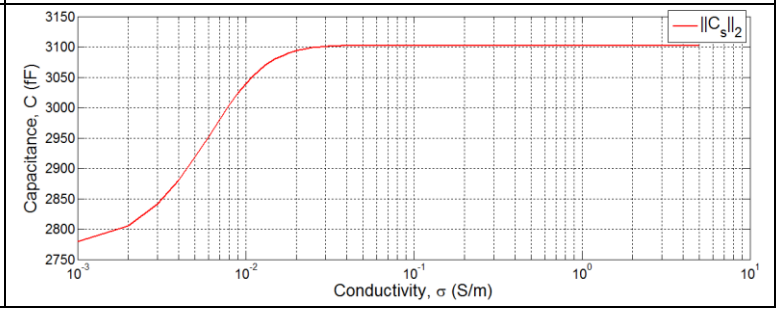

Difference of the measurements above $\|C_s - C_r\|_2$	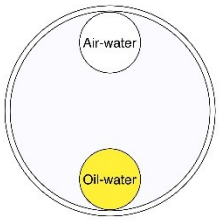	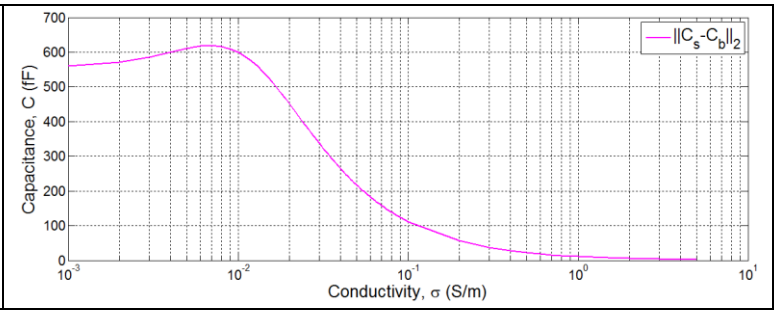

Table 9. Simulated capacitance changes when conductivity increases from 0 to 5 *S/m* (water background)

For image reconstruction, the difference of the measurements determines the quality of the image. In the third column of the Table 9, the value of the difference drops rapidly to approach the 0, which is much smaller than the value of low conductivity, i.e., less than 0.5 *S/m*. The big change in the 2-norm value of the difference value causes decline in image quality. Several points within the conductivity range from 0 to 0.1*S/m* are selected to reconstruct the images, and the capacitance measurement of the 5*S/m* is also shown in Table 10.

2-norm value plot along σ changes	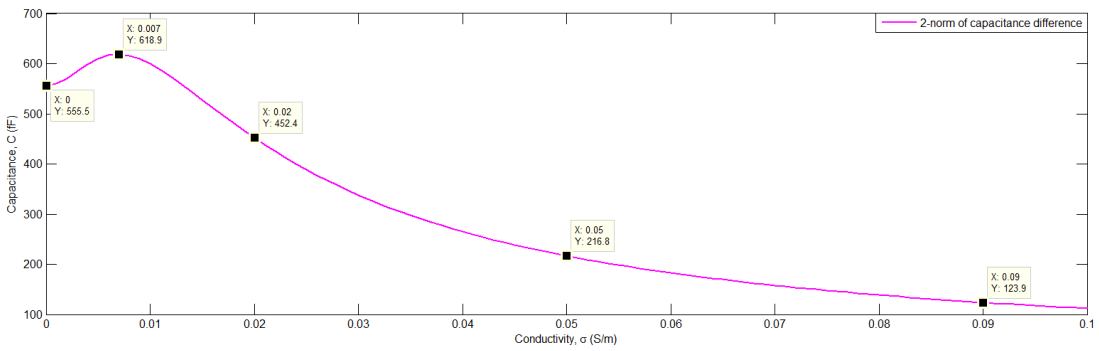		
σ (*S/m*)	0	0.007	0.02
ECT images	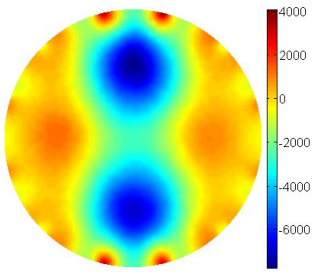	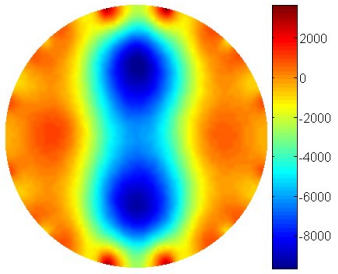	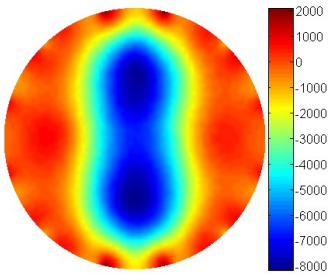
σ (*S/m*)	0.05	0.09	5
ECT images	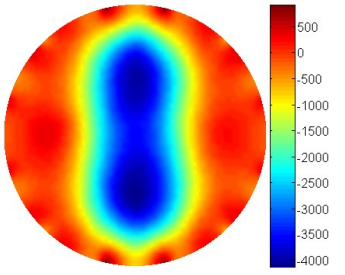	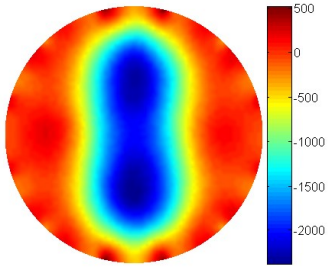	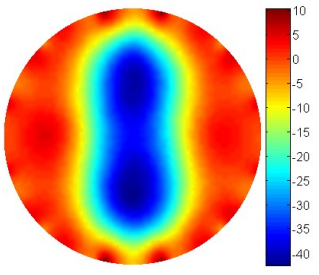

Table 10. ECT images reconstructed by the selected simulated capacitance (water background)

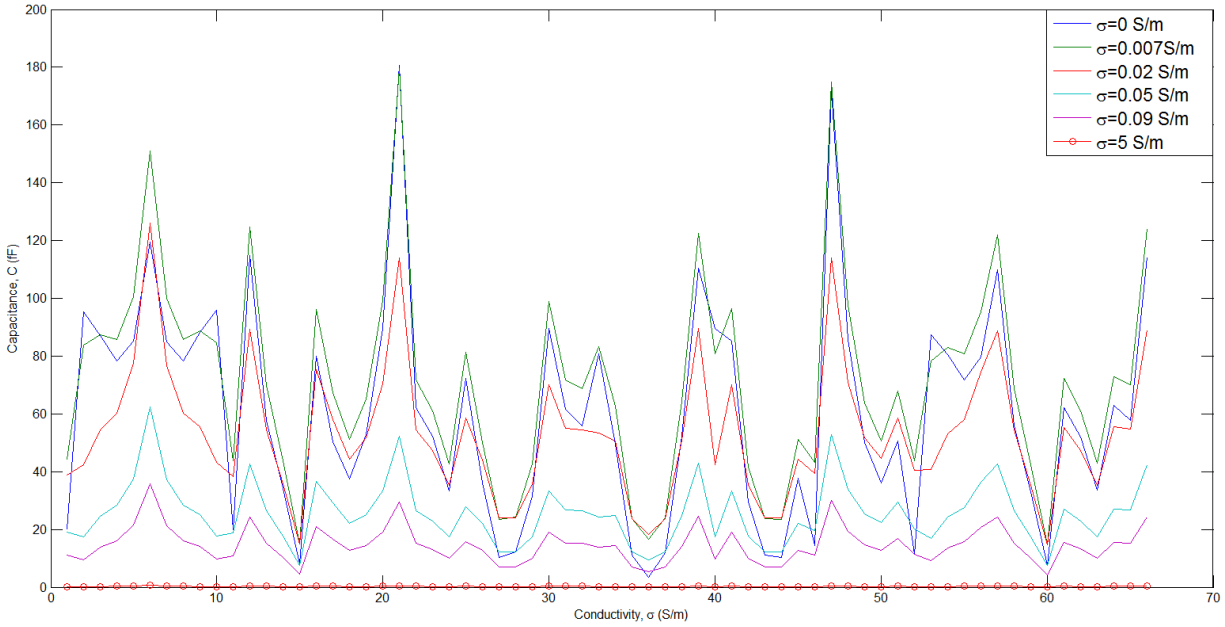

Figure 5. Six sets of inter-electrode capacitances change, $|C_S - C_T|$, from simulation

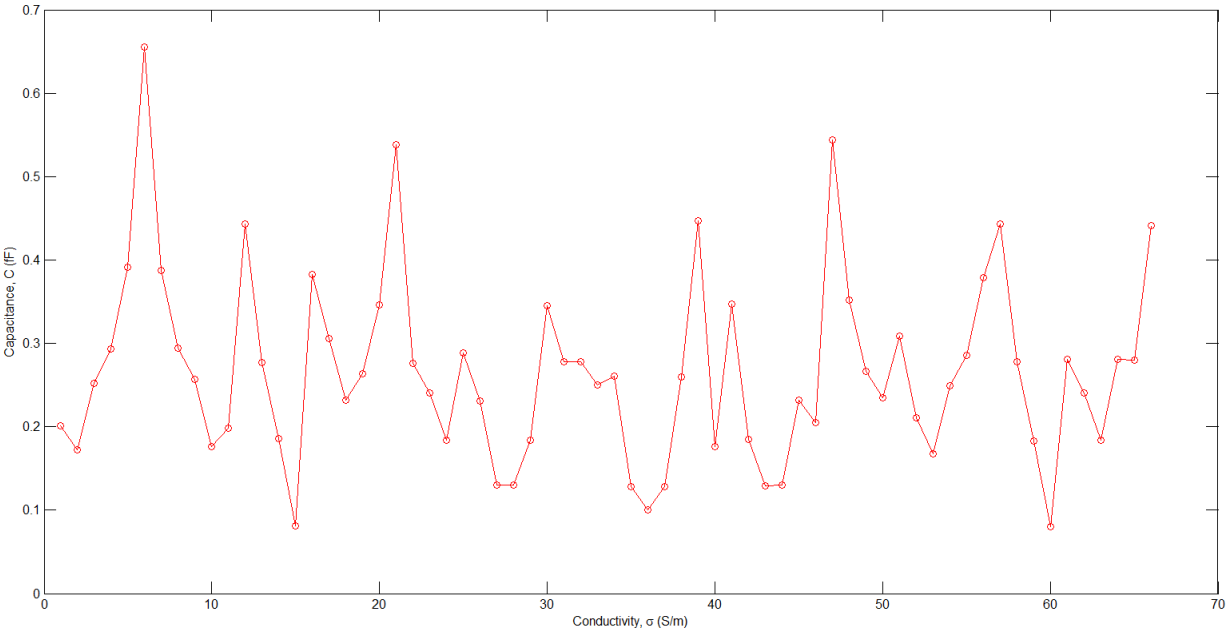

Figure 6. Inter-electrode capacitances change, $|C_S - C_T|$ when conductivity is 5*S/m*

The simulated inter-electrode capacitance changes at 6 selected values of conductivity are plotted in Figure 5. As the conductivity increases, the capacitance difference declines and is less sensitive to permittivity distribution. However in Figure 6, the profile of these plots remains very similar, even the conductivity reaches 5 *S/m*. Therefore, the reconstruction image at 5 *S/m* indicates a very similar pattern to the one at 0.09 *S/m*. But calculated permittivity values of each case are in difference scale, which can be found by the colour bars in Table 10.

5.1.2 Experimental results

The bottom of the sensor pipe is sealed, so it can be filled with water for this test. The experiment starts with measuring DI water ($\sigma_{DI} = 2.87 \times 10^{-4} S/m$). Then the conductivity is increased to 0.5450 *S/m* by adding high-concentration saline water slowly and gradually. Both conductivity and the inter-capacitance are measured and recorded. For the capacitance measurements, as the simulations in Table 9, the water-filled sensor is measured as the reference, C_r; the bottles of air and oil are placed at top and bottom within the sensor region are the sample measurement, C_s. In Figure 7, the 2-norms of the capacitances difference are plotted.

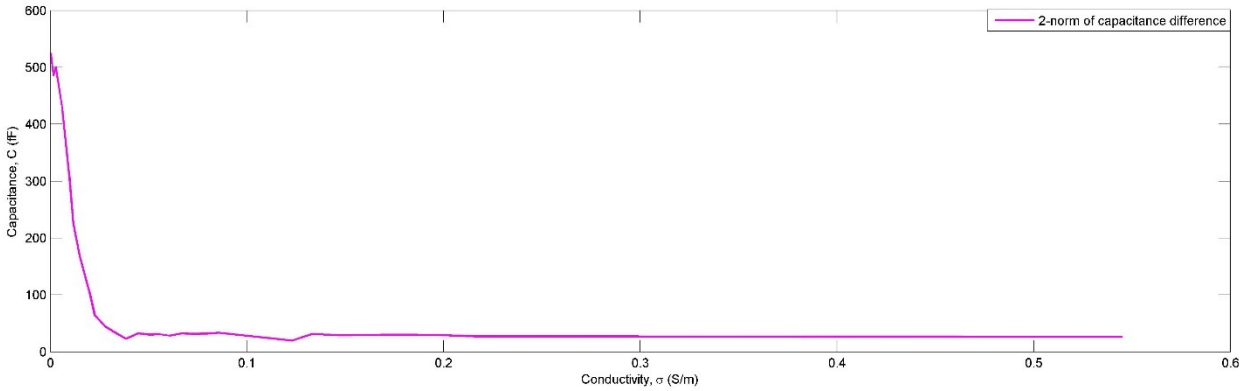

Figure 7. 2-norm of the capacitance measurement difference between reference and samples, Cr-Cs

To compare with images reconstructed from simulated measurements in Table 9, the experimental measurement are calculated and the images are plotted in Table 11. The points close to the one selected in Table 9 are chosen. And the imaging fails around $\sigma = 0.3\ S/m$ and an image at the 0.5450 is shown at the end of Table 11.

2-norm value plot along σ changes	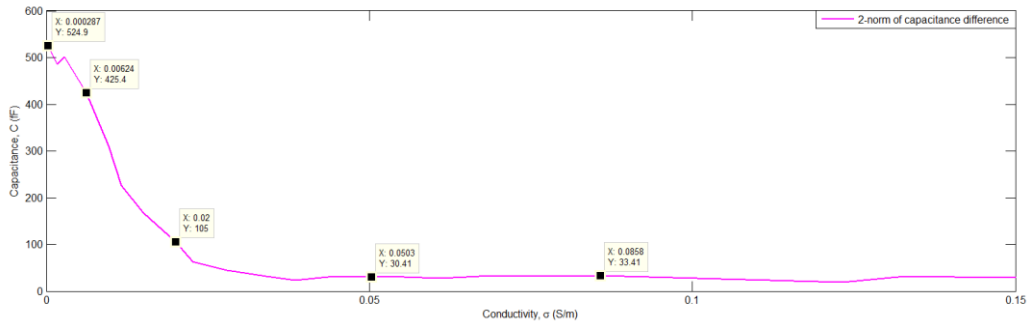		
σ (*S/m*)	0.0003	0.0062	0.0200

ECT images	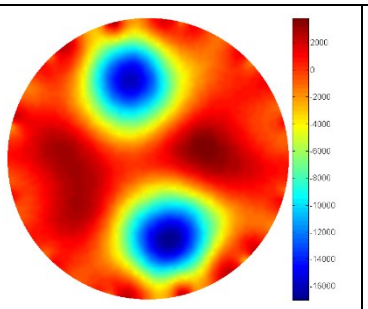	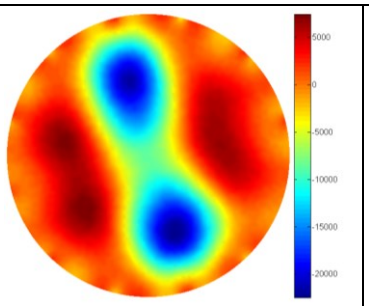	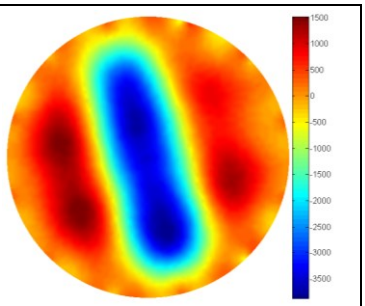
σ (*S/m*)	0.0503	0.0858	0.5450
ECT images	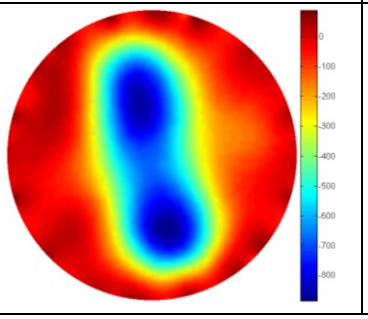	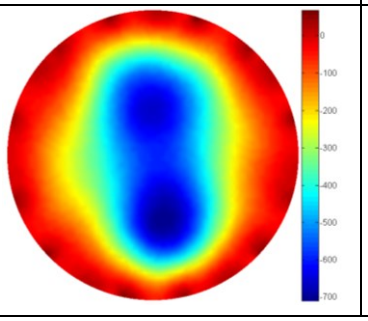	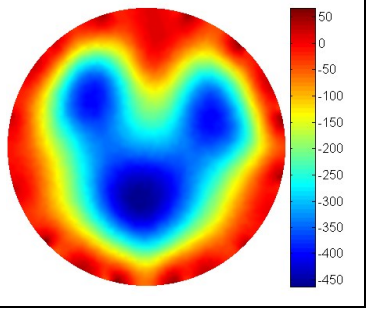

Table 11. ECT images reconstructed by the selected measured capacitance (water background)

5.2 Dual modality test

5.2.1 Positions of samples in water

The conductivity of the water background are chosen as 0.863 *S/m* and 1.557 *S/m* (9% saline water). The other two-phase flow is simulated by a bottle of silicone oil and a bottle of air. The samples are placed in the positions below in Table 12.

Position
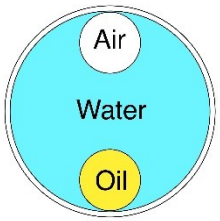

Table 12. Positions of the samples in water

5.2.2 MIT experiments

The conductivity difference between the background and samples determines the ability of MIT to image the dielectric from the conductive inclusions. From our experiments and observation, when the conductivity of the water background is lower than 0.5*S/m*, the MIT images starts deforming, and our MIT system reaches its limitation of detecting non-conductive samples from conductive background.

	0.863*S/m*	1.557 *S/m*

MIT images	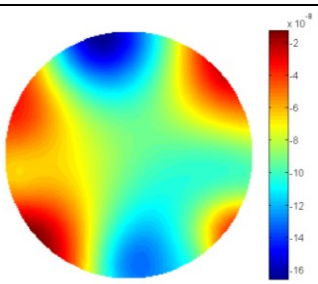	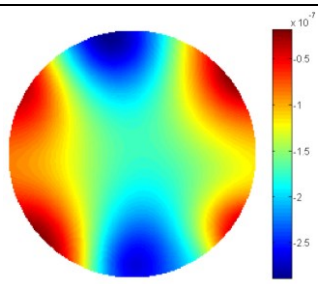

Table 13. MIT images of air and oil samples under difference conductive background

5.2.3 ECT experiments

The images of ECT under different conductivity water background are listed in Table 14. The letter "r" in the table is the regulation factor in Tikhonov algorithm, and the images on the same column are calculated by the same settings of Tikhonov parameters. In the column of **ECT (air reference)**, the air-fully-filled sensor is measured as a reference measurement. ECT can only image the two low-permittivity inclusions clearly under the DI water background. As the conductivity goes a little bit higher, the reconstruction image fails. In the column of **ECT (water reference)**, the water-fully-filled sensor is measured as a reference measurement, which is changing as the conductivity changes. The image quality deteriorates while conductivity increase, but it performs better than the air reference.

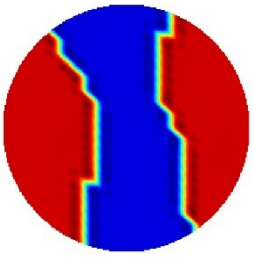

Figure 8. Binary image of threshold of 55% of the maximum value over the MIT image.

However, due to the limitation of our current equipment, the conductivity contrast lower than 0.5*S/m* cannot be imaged by MIT. Theoretically

Therefore we use the images of the conductivity contrast of 1.557*S/m* from Table 13 as a guidance to modify the sensitivity map of ECT, and by setting up a threshold of 55% of the maximum value on this image, a binary image as in Figure 8 is obtained, and in the following ECT process, this image provides the information of dielectric samples and assist ECT to generate a new forward model to help ECT to separate dielectric samples.

In the last column, **MIT-ECT**, the reference measurements are the same as the column of **ECT (water reference)**, but the sensitivity map has been updated with the image from MIT (Figure 8). The image quality maintained where the other two fails.

Modality / Conductivity	ECT (air reference)	ECT (water reference) r=1e-8	MIT-ECT r=1e-5
0.0003 *S/m* (DI water)	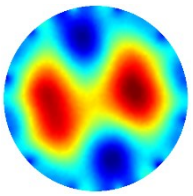	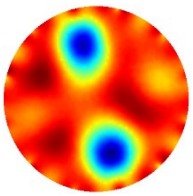	N/A
0.0097 *S/m*	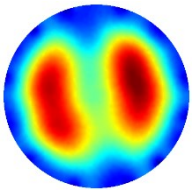	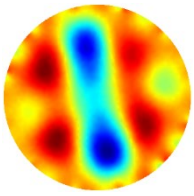	N/A
0.0200 *S/m*	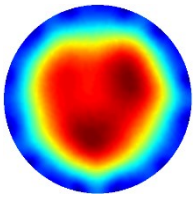	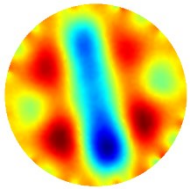	N/A
0.0586 *S/m* (Tap water)	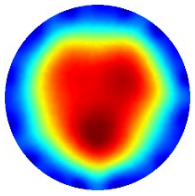	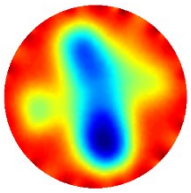	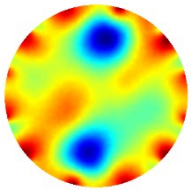
0.1318 *S/m*	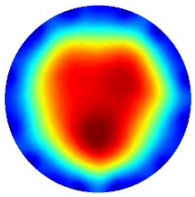	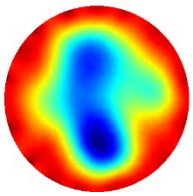	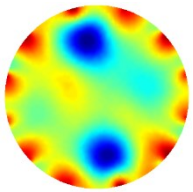
0.1958 *S/m*	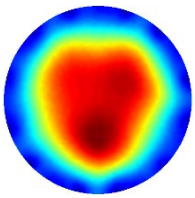	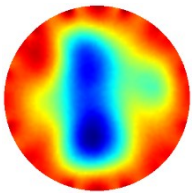	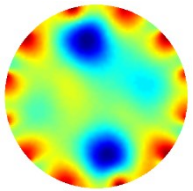
0.3060 *S/m*	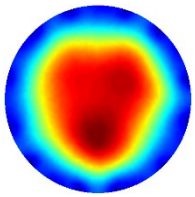	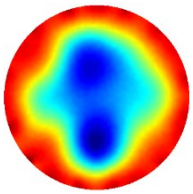	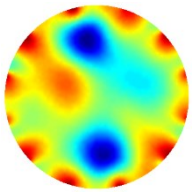
0.5450 *S/m*	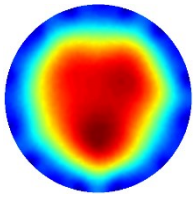	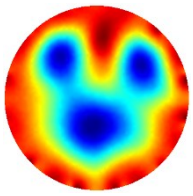	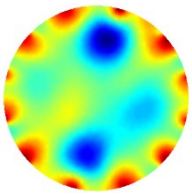

Table 14. Reconstruction images of three-phase-system, water background

6. Discussion

The dual-modality raised in this paper is a sequential method to image the region containing both conductivity and permittivity contrasts. MIT is sensitive to conductive phase, and as such can be used to distinguish conductivity contrast. The conductivity contrast can be formed either by using a conductive inclusion in a non-conductive background or a non-conductive inclusion in a conductive background. In the context of this study, we considered two representative and also common backgrounds in three-phase flow imaging, i.e., a free space and a water background scenarios in the testing environment. The core-concept of dual modality method is to provide a priori knowledge of the conductivity distribution through the use of MIT, and then to use this information by ECT in attempt to resolve permittivity contrast, hence a three-phase distribution can be established.

Although MIT has a proved capability to identify conductivity contrast [5], the response of MIT system alters according to the change of background conductivity, which suggests for each scenarios mentioned above, different imaging capabilities are observed. Among a large quantity and qualitative experiments conducted, it is showed that in a water background, a conductivity contrast as small as 0.5*S/m* can be resolved, which occupies 5.38% of the total imaging region in area. In addition, for an inclusion occupying the same percentage of the imaging region, a conductivity contrast of about 1 *S/m* is resolved in a free space background. Based on these findings, we anticipate that for both scenarios, for any conductivity contrast lower than these, ECT could be able to operate.

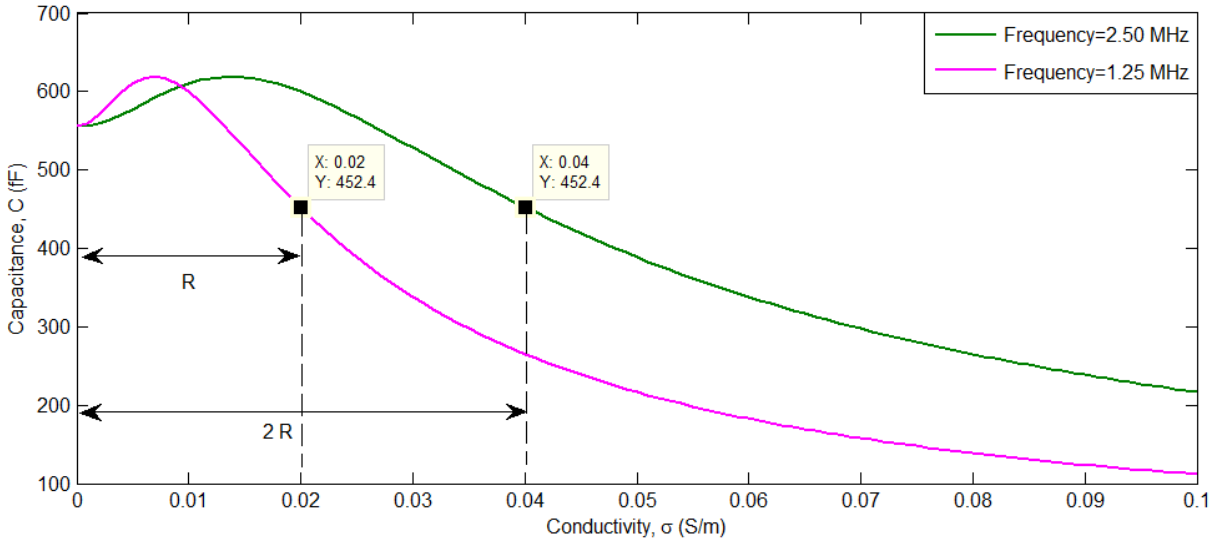

Figure 9. Conductivity and frequency impact on the capacitance measurement

From the conductivity test on the water-background scenario, a conductivity contrast of 0.02 *S/m* is regarded as a detection limitation of ECT. Under this value, ECT can separate the two low-permittivity phases, i.e., oil and air. From equation (5), the complex permittivity is defined as the equation below.

$$\varepsilon_{complex} = \varepsilon(x) + \frac{\sigma(x)}{i\omega} \quad (13)$$

Therefore the factor that impacts the imaginary part of this complex value is not only the conductivity but also the signal frequency of the measurement unit. Mathematically, the detection limits can be extended over 0.02*S/m* by increasing the frequency. In Figure 9, the capacitance detection range is doubled when the frequency is doubled, which is generated by the complex ECT model. However, due to lack of a higher frequency measurement unit, this extension of limit cannot be proved experimentally. If this mathematical induction works, by increasing signal frequency, the limit of conductivity of ECT can reaches the limit of MIT, and dual modality would work on this scenario as well as the air-background tests.

7. Conclusion

Preliminary results demonstrate the feasibility of three phase flow imaging using a dual modality MIT-ECT combination. The main results in this paper are focusing on free space background where the effect of conductivity in ECT is minimal and the MIT provides information on location and size of water inclusion, which represents the high permittivity component in ECT, by incorporating this in ECT forward model and the ECT reference measurement, the two low contrast component can be separated. With the case of de-ionized water MIT could not help and further work will be done this dual modality with the conductive backgrounds. Although it requires direct contact, the ERT can image the conductive phase with conductive background. Further development in ECT-MIT combination for conductive background will be subject of further research.

References

1. Xie, C.G., et al., *Electrical capacitance tomography for flow imaging: system model for development of image reconstruction algorithms and design of primary sensors.* Iee Proceedings-G Circuits Devices and Systems, 1992. **139**(1): p. 89-98.
2. Warsito, W. and L.S. Fan, *Measurement of real-time flow structures in gas–liquid and gas–liquid–solid flow systems using electrical capacitance tomography (ECT).* Chemical Engineering Science, 2001. **56**(21–22): p. 6455-6462.
3. Jeanmeure, L.F.C., et al., *Direct flow-pattern identification using electrical capacitance tomography.* Experimental Thermal and Fluid Science, 2002. **26**(6-7): p. 763-773.
4. Jaworski, A.J. and T. Dyakowski, *Application of electrical capacitance tomography for measurement of gas-solids flow characteristics in a pneumatic conveying system.* Measurement Science & Technology, 2001. **12**(8): p. 1109-1119.
5. Watson, S., et al., *A magnetic induction tomography system for samples with conductivities below 10 S m −1.* Measurement Science and Technology, 2008. **19**(4): p. 045501.

6. Wei, H.-Y. and M. Soleimani, *Two-phase low conductivity flow imaging using magnetic induction tomography.* Progress In Electromagnetics Research, 2012. **131**: p. 99-115.
7. Thorn, R., G.A. Johansen, and B.T. Hjertaker, *Three-phase flow measurement in the petroleum industry.* Measurement Science and Technology, 2013. **24**(1): p. 012003.
8. Deng, X. and W. Yang, *Fusion research of electrical tomography with other sensors for two-phase flow measurement.* Measurement Science Review, 2012. **12**(2): p. 62-67.
9. Qiu, C., B. Hoyle, and F. Podd, *Engineering and application of a dual-modality process tomography system.* Flow Measurement and Instrumentation, 2007. **18**(5): p. 247-254.
10. Chaminda, P., et al., *Electrical capacitance tomography (ECT) and gamma radiation meter for comparison with and validation and tuning of computational fluid dynamics (CFD) modeling of multiphase flow.* Measurement Science and Technology, 2014. **25**(7): p. 075404.
11. Hjertaker, B.T., R. Maad, and G.A. Johansen, *Dual-mode capacitance and gamma-ray tomography using the Landweber reconstruction algorithm.* Measurement Science and Technology, 2011. **22**(10): p. 104002.
12. Zhang, M., L. Ma, and M. Soleimani, *Magnetic induction tomography guided electrical capacitance tomography imaging with grounded conductors.* Measurement, 2014. **53**(0): p. 171-181.
13. Cheney, M., D. Isaacson, and J.C. Newell, *Electrical impedance tomography.* SIAM review, 1999. **41**(1): p. 85-101.
14. Soleimani, M., *Computational aspects of low frequency electrical and electromagnetic tomography: A review study.* International Journal of Numerical Analysis and Modeling, 2008. **5**(3): p. 407-440.
15. Yang, W.Q. and L.H. Peng, *Image reconstruction algorithms for electrical capacitance tomography.* Measurement Science & Technology, 2003. **14**(1): p. R1-R13.
16. Dyck, D.N., D.A. Lowther, and E.M. Freeman, *A method of computing the sensitivity of electromagnetic quantities to changes in materials and sources.* Ieee Transactions on Magnetics, 1994. **30**(5): p. 3415-3418.
17. Somersalo, E., D. Isaacson, and M. Cheney, *A linearized inverse boundary-value problem for maxwell equations.* Journal of Computational and Applied Mathematics, 1992. **42**(1): p. 123-136.
18. Soleimani, M. and W.R.B. Lionheart, *Nonlinear image reconstruction for electrical capacitance tomography using experimental data.* Measurement Science & Technology, 2005. **16**(10): p. 1987-1996.
19. Wei, H.-Y. and M. Soleimani, *Hardware and software design for a National Instrument-based magnetic induction tomography system for prospective biomedical applications.* Physiological Measurement, 2012. **33**(5): p. 863.
20. Peyman, A., C. Gabriel, and E.H. Grant, *Complex permittivity of sodium chloride solutions at microwave frequencies.* Bioelectromagnetics, 2007. **28**(4): p. 264-274.